materials

MDPI

Article

Preparation of MoS_2 Nanospheres using a Hydrothermal Method and Their Application as Ammonia Gas Sensors Based on Delay Line Surface Acoustic Wave Devices

Chan-Yu Chung [1], Ying-Chung Chen [1,2], Feng-Renn Juang [1], Kuo-Sheng Kao [3,*] and En-I Lee [1]

[1] Department of Electrical Engineering, National Sun Yat-Sen University, Kaohsiung 80424, Taiwan; d063010001@student.nsysu.edu.tw (C.-Y.C.); ycc@mail.ee.nsysu.edu.tw (Y.-C.C.); frjuang@mail.ee.nsysu.edu.tw (F.-R.J.); m103010093@student.nsysu.edu.tw (E.-I.L.)
[2] College of Semiconductor and Advanced Technology Research, National Sun Yat-Sen University, Kaohsiung 80424, Taiwan
[3] Department of Computer and Communication, SHU-TE University, Kaohsiung 82445, Taiwan
* Correspondence: kks@stu.edu.tw

Abstract: An ammonia sensor based on a delay-line surface acoustic wave (SAW) device is developed in this study by coating the delay line area of the device with a nano-structured molybdenum disulfide (MoS_2) sensitive material. A SAW device of 122 MHz was designed and fabricated with a pair of interdigital transducers (IDTs) defined on a 128° y-cut $LiNbO_3$ substrate using photolithography technologies, and the aluminum IDT electrodes were deposited by a DC magnetron sputtering system. By adjusting the pH values of precursor solutions, molybdenum disulfide (MoS_2) nanospheres were prepared with various structures using a hydrothermal method. Finally, an NH_3 gas sensor with high sensitivity of 4878 Hz/ppm, operating at room temperature, was successfully obtained. The excellent sensitivity performance may be due to the efficient adsorption of NH_3 gas molecules on the surfaces of the nanoflower-like MoS_2, which has a larger specific surface area and provides more active sites, and results in a larger change in the resonant frequency of the device due to the mass loading effect.

Keywords: SAW; MoS_2; NH_3; gas sensor; nanosphere

Citation: Chung, C.-Y.; Chen, Y.-C.; Juang, F.-R.; Kao, K.-S.; Lee, E.-I. Preparation of MoS_2 Nanospheres using a Hydrothermal Method and Their Application as Ammonia Gas Sensors Based on Delay Line Surface Acoustic Wave Devices. *Materials* **2023**, *16*, 4703. https://doi.org/10.3390/ma16134703

Academic Editor: Cristian E. Simion

Received: 24 May 2023
Revised: 17 June 2023
Accepted: 21 June 2023
Published: 29 June 2023

1. Introduction

The development and application of industrial technology have improved the convenience of human life, but they have also brought many new challenges, such as negative impacts on air quality and the ecological environment. There are many kinds of pollutants in the air, among which the dust-like particles floating in the air are called particulate matter (PM). When the suspended particulate matter is $PM_{2.5}$ (particle size less than or equal to 2.5 microns), it can penetrate the bubbles in the lungs and cause serious harm to human health as the blood circulates in the body, which cannot be ignored. It has been clarified that the main source precursors of $PM_{2.5}$ are sulfur dioxide, nitrogen oxides, ammonia, etc. [1,2]. The US Occupational Safety and Health Administration (OSHA) has declared that the acceptable average ammonia exposures time is 8 h at 25 ppm and 15 min at 35 ppm [3,4]. If the human body strongly inhales high concentrations of NH_3, various symptoms such as tearing, coughing, and dyspnea will appear, and death can be caused under extremely high concentrations of ammonia [5,6].

Ammonia gas (NH_3) is commonly used in industrial manufacturing processes. However, when the concentration of NH_3 in the air reaches a certain range, of about 15% to 28%, it is explosive. Many kinds of NH_3 sensors using various sensitive materials have been developed. For example, metal-oxide sensors, which are current research hotspots, have the advantages of simple operation, low cost, and fast response, but complex synthesis processes and higher operating temperatures are required for better performance, and

because of high power needed, their application in the Internet of Things is bound to be limited [7–11]. Therefore, there is an urgent need to study high-performance NH_3 sensors operating at room temperature for immediate preventive measures under adverse conditions.

In this study, a SAW device was employed to perform as an ammonia sensor using novel nanostructured molybdenum disulfide (MoS_2) as the sensitive layer. In the application of gas sensors, surface acoustic wave devices have the advantages of high sensitivity, low detection limit and operation at room temperature, which can be used to measure the trace concentrations [12–14]. In addition, the frequency responses of SAW sensors can support wireless sensing, and also have outstanding performance at room temperature [15].

The resonant frequency f of a surface acoustic wave device is related to the spacing of the interdigital transducer (IDT) electrodes and the wave velocity, with the relationship of $f = \upsilon/\lambda$ where υ is the wave velocity, λ is the wavelength, and f is the resonant frequency. The 4 times the line width of the electrode (d) can excite the acoustic wave, with a wavelength of $\lambda = 4d$. In the design of a SAW gas sensor, the delay line area of the SAW device is coated with a sensitive thin film, and the gas molecules are adsorbed through the sensitive thin film to produce physical changes, which will change the resonant frequency of the SAW device [16,17].

Molybdenum disulfide (MoS_2) has a large band gap, a layered structure, semiconductor characteristics, etc. It is an excellent gas-sensing material, with high sensitivity and selectivity when applied as a sensor [18,19]. In addition, studies have shown that the shape, size, and specific surface area of gas-sensing materials also have a great influence on the gas-sensing performance [20]. Therefore, it is of great significance to study the gas-sensing properties of MoS_2 with different morphologies for the design of sensor structures. In this study, three kinds of ammonia sensors with different MoS_2 morphologies were constructed based on the hydrothermal method, and the gas-sensing properties of MoS_2 with three different morphologies for ammonia gas were studied.

2. Materials and Methods

2.1. Preparation of Molybdenum Disulfide Nanospheres

In this study, MoS_2 nanospheres, prepared with a simple hydrothermal method, were used as the sensitive materials of the surface acoustic wave gas sensors. Briefly, Na_2MoO_4 (0.05 M) and C_2H_5NS (0.15 M) were added to 40 mL of deionized (DI) water and stirred for 30 min to fully dissolve. In order to obtain different MoS_2 morphologies, various amounts of HCl were added to adjust the pH values of the solutions, with pH1, pH3, and pH5, respectively, and were then stirred for 10 min to form uniform precursor solutions. Subsequently, the precursor solution was poured into 100 mL of Teflon liner, then loaded into an autoclave reactor and heated to 180 °C in a high-temperature furnace for 20 h. Finally, the obtained powders were washed several times by centrifuge with ethanol and deionized water. After drying at 80 °C for 6 h on a heater platform, various morphologies of MoS_2 nanospheres were obtained. The process flow of the hydrothermal method is shown in Figure 1.

2.2. Fabrication of Surface Acoustic Wave Devices

$LiNbO_3$ is a crystal that integrates multiple effects such as piezoelectricity, electro-optic, and nonlinear optics, and has the advantages of high temperature resistance and corrosion resistance. In this study, 128° y-cut $LiNbO_3$ was adopted as the piezoelectric substrate with a wave speed of ≈3900 m/s. The line width of the interdigital transducer (IDT) electrodes of 8 μm was designed to excite the surface acoustic wave with a wavelength of 32 μm, which resulted in a resonant frequency of 122 MHz. Figure 2 shows the fabrication processes of a SAW device. Firstly, the 128° y-cut $LiNbO_3$ substrate was cleaned according to the RCA cleaning processes, and then the photoresist (AZ1500) (1.2 μm) was coated on the substrate using a spinning coater, and heated on a heater platform for soft baking, and then exposed and developed through the usual photolithography processes. In this study, a dual-target DC sputtering system was used to deposit Ti (20 nm) and Al (100 nm) as IDT

electrodes, in which the titanium metal film was used as an adhesive layer. The advantage of the double-target sputtering system is that it can continuously deposit multi-layer films without restarting the vacuum chamber, avoiding pollution or oxidation on the films. Therefore, a high-quality SAW device can be obtained through controlling the film quality. Finally, the lift-off process was carried out by immersing the substrate into the acetone solution and shaking using an ultrasonic washing machine to remove the photoresist and unnecessary films to complete the SAW device.

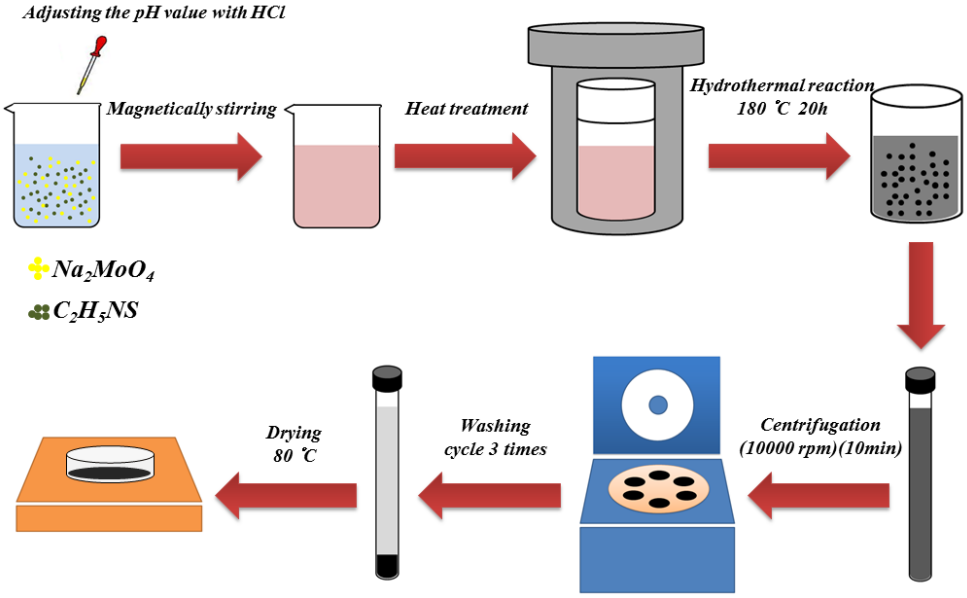

Figure 1. Process flow of the hydrothermal method to prepare MoS_2 nanospheres.

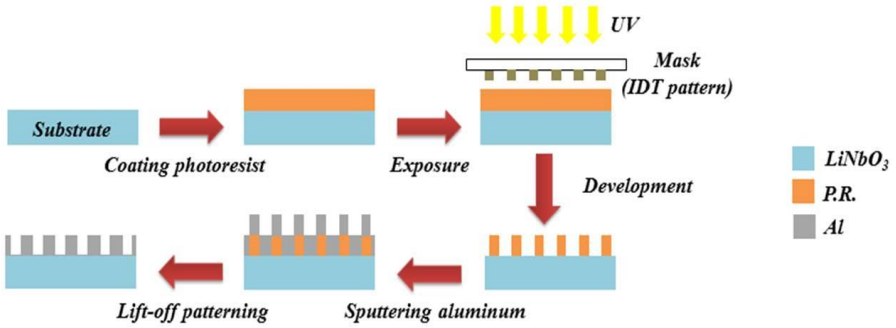

Figure 2. Fabrication processes of a surface acoustic wave device [21].

2.3. Sensor Fabrication

In this study, a SAW delay line structured device with a resonant frequency of 122 MHz was successfully fabricated on the 128° y-cut $LiNbO_3$ substrate. Then, the MoS_2 nanospheres, as the sensitive materials, were spin-coated on the delay line area of the SAW devices. Figure 3 shows the preparation processes of the sensitive layer of the sensor. First, the IDT electrodes of the SAW device were covered with tape. Then, the MoS_2 powders were mixed with absolute ethanol at a weight ratio of 1:30, and stirred for 20 min. Then, the MoS_2 solution of 1 mL was dropped on the delay line area using a precision dropper, and spun at 1200 rpm for 30 s. Finally, the substrate and the sensitive materials were dried at 90 °C for 6 min. After removing the tape, the sensor device was fabricated. Figure 4 is a schematic diagram of the complete ammonia gas sensor. The SPB-U668 aluminum wire bonder was adopted to connect the SAW sensor and the microstrip line, according to the design rules of the coplanar waveguide (CPW) microstrip line and the impedance calculation of the 50 ohm (PCB) board.

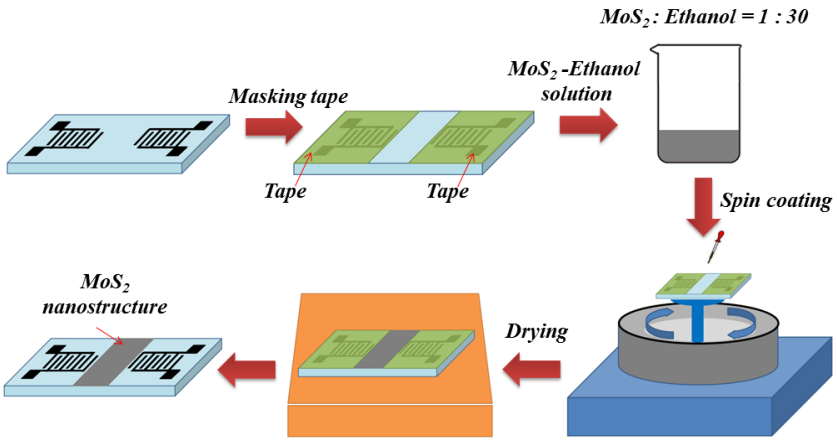

Figure 3. Fabrication flow chart of a SAW gas sensor based on MoS_2 nanospheres.

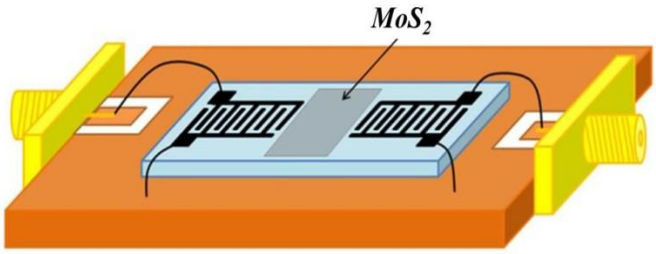

Figure 4. Schematic of the complete ammonia gas sensor.

2.4. Material Analysis and Sensor Measurement

The nanostructures of MoS_2 will affect the properties of the sensor devices. Therefore, scanning electron microscopy (SEM, JEOL-6700 field emission SEI/BEI type, JEOL, Ltd., Tokyo, Japan), energy-dispersive X-ray spectroscopy (EDX, JEOL, Ltd., Tokyo, Japan), and X-ray diffraction (XRD, Bruker, Billerica, MA, USA) were used to analyze the nanostructures and atomic ratio of MoS_2 under different hydrothermal conditions. The frequency response of the SAW sensor was measured using the P9372A Keysight Streamline USB Vector Network Analyzer (Keysight, Santa Rosa, CA, USA).

Gas sensing measurements were performed on a static gas sensing measurement system at room temperature. During the test, a 25% ammonia solution was carried by N_2 gas and injected into the vaporizer through a micro-syringe, then mixed with air in a 3 L test chamber to prepare NH_3 gas with various concentrations of 5–50 ppm. Finally, the desired concentration of NH_3 gas was introduced into the measurement chamber, and the frequency response of the sensor exposed to different concentrations of NH_3 gas was recorded by the network analyzer.

3. Results and Discussion

3.1. Performance of the Designed Surface Acoustic Wave Device

The performance of a SAW device can be defined by its figure of merit (*FoM*), as in Equation (1).

$$FoM = Q \times K^2 \tag{1}$$

where Q is the quality factor, and K^2 is the electromechanical coupling factor of the SAW device. Besides, Q and K^2 can be derived from the following Equations (2) and (3).

$$Q = \frac{f_0}{f_H - f_L} \tag{2}$$

$$K^2 = \frac{\pi}{4N} \times \frac{Ga}{B} \tag{3}$$

where f_0 is the center frequency of the SAW filter, f_H and f_L are the upper and low 3-dB frequencies of the SAW filter, respectively. B is the radiated susceptance; Ga is the radiated conductance; and N is the IDT pair number.

In practical applications, it is necessary to pursue SAW devices with high electromechanical coupling factors (K^2) and quality factors (Q). However, there are some trade-offs between these two parameters. Therefore, *FoM* can better demonstrate the advantages and disadvantages of the device during the design process of SAW. In this study, the fabricated SAW device exhibited a Q factor of 180, K^2 of 3.29 % and *FoM* of 5.922.

3.2. Characteristic Analysis of Molybdenum Disulfide

In this experiment, by adjusting the pH values of the precursor solutions, various MoS_2 nanospheres were successfully prepared using the hydrothermal method. It is demonstrated that HCl will play an important role in the synthesis of MoS_2 [22]. Without HCl, the pH value of the precursor solution was about 6, and no MoS_2 powder was produced at this situation. As HCl was added into the precursor solution, MoS_2 appeared without any byproduct at pH value of 5. However, as the concentration of HCl increased further, the byproduct MoO_2 appeared at pH values of 3 and 1. The X-ray diffractions of obtained MoS_2 samples with different pH values were shown in Figure 5. It can be inferred that HCl may enhance the formation of MoS_2 and MoO_2.

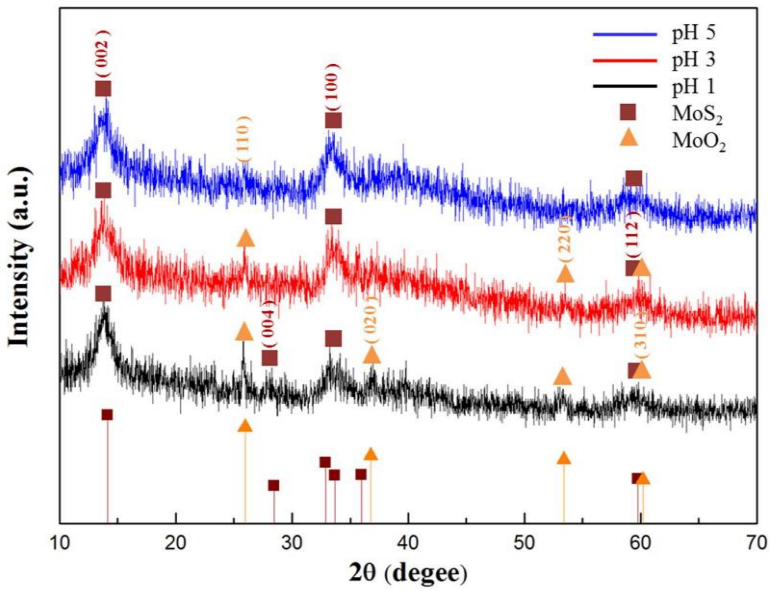

Figure 5. X-ray diffractions of MoS_2 samples obtained from precursor solutions with different pH values.

The concentration of HCl in the reaction solution not only affects the formation of MoS_2, but also has a great influence on the microscopic morphology. From the SEM images in Figure 6, it can be found that the nanospheres are formed by flake agglomeration. As the pH value increases, the flake structure becomes more obvious. When the pH value was 5, the structure resembled a nanosphere of a rose. The experimental results show that the morphological control of the product could be achieved by adjusting the concentration of HCl in the reaction solution.

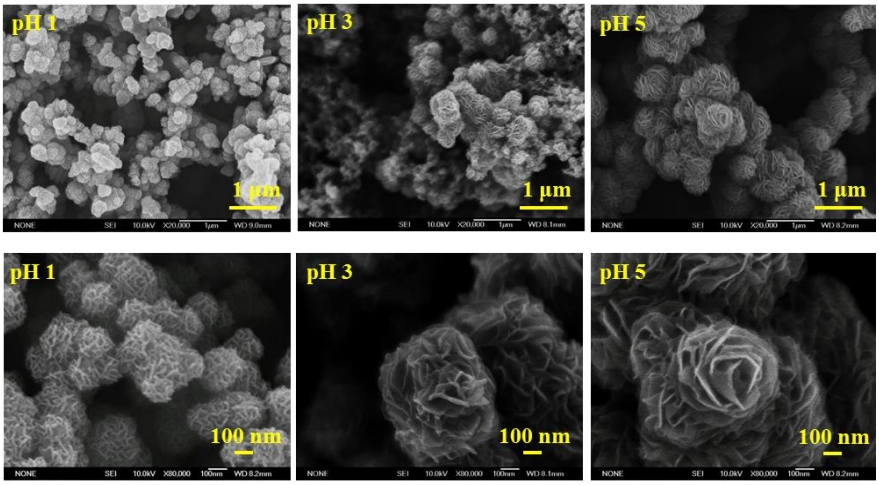

Figure 6. SEM images of MoS_2 microstructures obtained from precursor solutions with different pH values.

From the EDX analysis, it can be clearly observed that there were only Mo and S elements in the MoS_2 samples without impurities. Moreover, as the pH value approached neutral, the atomic ratio of Mo and S approached 1:2, as shown in Table 1.

Table 1. EDX analysis of MoS_2 nanospheres obtained from various precursor solutions.

Precursors	***pH1***	***pH3***	***pH5***
Element	*Atomic %*	*Atomic %*	*Atomic %*
S	61.32	65.24	67.57
Mo	38.68	34.76	32.43
Atomic ratio (S/Mo)	1.59	1.88	2.08

3.3. Analysis of Ammonia Gas Sensor

The MoS_2 nanospheres obtained from various precursor solutions with pH values of pH1, pH3, and pH5 were coated on the delay line area as the sensitive layers of the SAW gas sensors, and those were defined as sensor−1, sensor−2, and sensor−3. As the gas sensors were exposed to different concentrations of NH_3, variations in the frequency response could be observed and shown in Figure 7a for sensor−1, 8a for sensor−2, and 9a for sensor−3. For clarity, the sensor response near the resonant frequency of 122 MHz was zoomed in further, as shown in Figures 7b, 8b and 9b.

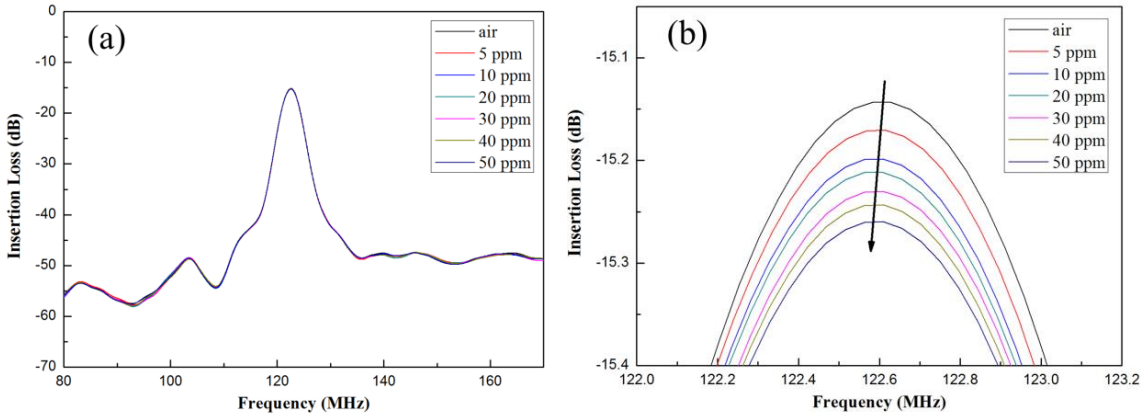

Figure 7. (**a**) Frequency variations at different ammonia concentrations for sensor−1. (**b**) Zoomed in near the region of 122 MHz resonant frequency.

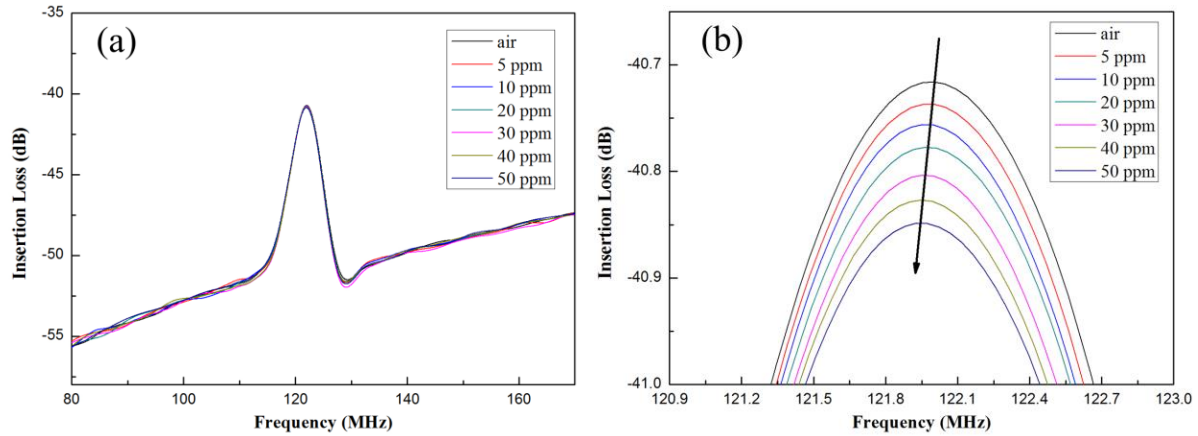

Figure 8. (**a**) Frequency variations at different ammonia concentrations for sensor−2. (**b**) Zoomed in near the region of 122 MHz resonant frequency.

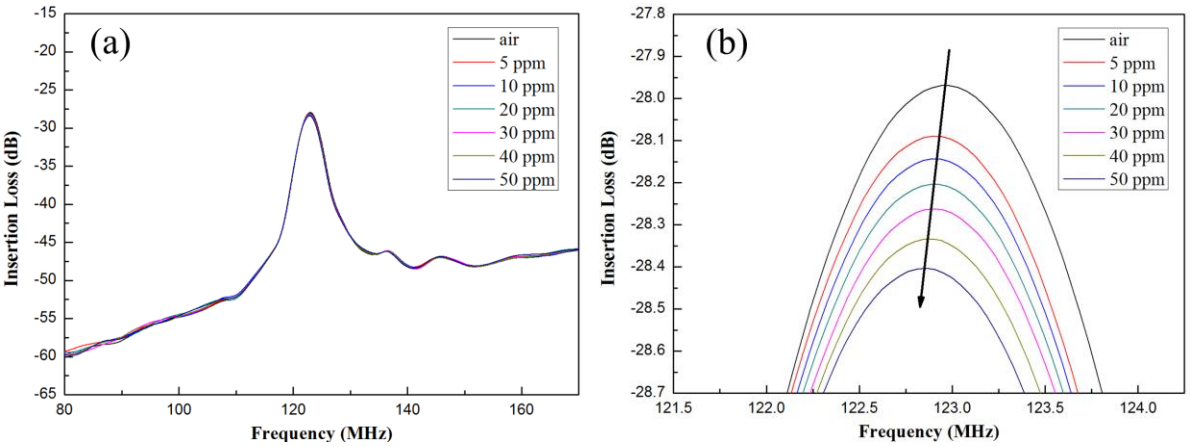

Figure 9. (**a**) Frequency variations at different ammonia concentrations for sensor−3. (**b**) Zoomed in near the region of 122 MHz resonant frequency.

The original resonant frequency of all sensors without NH_3 gas was around 122 MHz, whereas it shifted toward lower frequencies as the concentration of NH_3 gas increased. The frequency shifts for the three sensors are shown in Figure 10. Sensitivity is an important indicator of sensor performance, which refers to the ratio of sensor output variation to measured input variation; its calculation formula is as follows:

$$S = \frac{|f_0 - f_{gas}|}{\Delta c} \tag{4}$$

where S is the sensitivity, Δc is the change of gas concentration, f_0 is the frequency of the gas sensor in air, and f_{gas} is the frequency at which the gas sensor detects the measured gas. From Equation (4), the calculated sensitivities were 1402 Hz/ppm for sensor−1, 2816 Hz/ppm for sensor−2 and 4878 Hz/ppm for sensor−3, respectively. The detection limit could be as low as <1ppm.

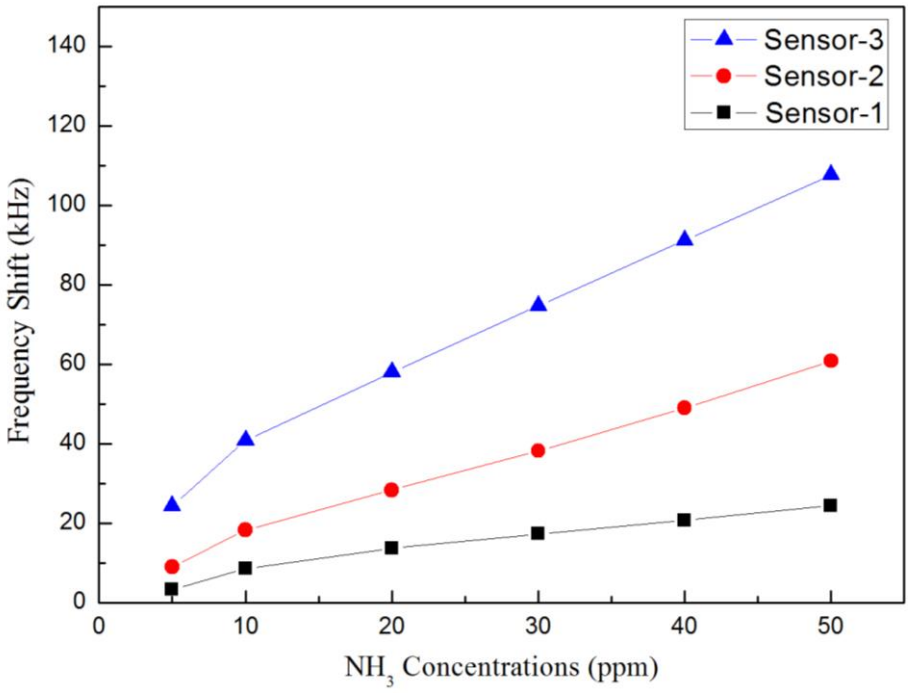

Figure 10. The frequency shifts of the fabricated sensors towards NH_3 gas concentrations.

In the SAW sensor, the resonant frequency change (Δf) may be related to mass loading or acoustoelectric interactions, or elastic changes when interacting with target gas molecules [23]. However, the lower value of the electromechanical coupling factor for 128° y-$LiNbO_3$-based SAW sensor is expected to result in a negligible contribution due to the acoustoelectric effect [24]. Therefore, the existence of acoustoelectric interaction can be ruled out in this case. Furthermore, it is essential to point out that mass loading causes the resonant frequency to move towards the lower end (i.e., decreasing the resonant frequency), while the elastic changes cause the resonant frequency to move towards the higher end (i.e., increasing the resonant frequency); that is, the material elasticity can also be ruled out and the change was negligible [24]. From the results obtained, it can be concluded that the frequency shift is owing to the mass loading effect.

The mass loading effect of a sensor can be expressed by the following formula [23–26]:

$$\Delta f = (k_1 + k_2) \times f_0^2 \times \Delta \rho s \quad (5)$$

where k_1 (-3.775×10^{-8} m^2 s kg^{-1}) and k_2 (-1.73×10^{-8} m^2 s kg^{-1}) are the material constants of 128° y−cut $LiNbO_3$ substrate. $\Delta \rho s$ is the density change of the sensing layer of the SAW sensor after being exposed to ammonia. Note that both k_1 and k_2 are negative, so a positive change in $\Delta \rho s$ results in a negative value in Δf [27–29].

In this study, sensor−3, prepared with MoS_2−pH5 as sensitive material, exhibited the best performance as an ammonia sensor. It is known from the literature that nanoflower−like MoS_2 has the highest specific surface area, and it is speculated that a larger specific surface area can provide more active sites, thereby obtaining higher ammonia gas−sensing response performances [30–33]. The resonant frequency of the SAW sensor shows a downward shift as the concentration of NH_3 increases. The frequency variation for 5–50 ppm NH_3 gas is shown in Table 2 for sensor−3, from which the sensitivity was calculated to be 4878 Hz/ppm. Compared with other works in the literature, this study showed an excellent sensitivity performance [34–38], as shown in Table 3.

Table 2. Resonant frequency and frequency shifts with different concentrations of NH_3 for fabricated MoS_2/SAW sensor−3.

Concentration of NH_3 (in ppm)	*Resonant Frequency (in MHz)*	*Shift in Frequency (in kHz)*
0	122.956197	Reference
5	122.931808	24.389
10	122.915316	40.881
20	122.898117	58.08
30	122.881384	74.813
40	122.864918	91.279
50	122.848529	107.668

Table 3. Comparisons of NH_3 sensing performance of SAW−based sensors with various sensing materials.

Working Frequency (MHz)	*Sensing Material*	*Sensitivity (Hz/ppm)*	*Ref.*
100	SnO_2/Co_3O_4	3.33	[34]
200	SiO_2-SnO_2	210	[35]
200	SiO_2-TiO_2	2000	[36]
200	AlO(OH)	154	[37]
200	TiO_2	500	[38]
122	MoS_2	4878	Present work

4. Conclusions

In this study, SAW devices of 122 MHz were fabricated using the piezoelectric 128° y−cut $LiNbO_3$ as the substrate. MoS_2 nanospheres were prepared using the hydrothermal method and coated on the delay line area of SAWs. Finally, an NH_3 gas sensor with a high sensitivity of 4878 Hz/ppm was successfully obtained. The reason for the improved sensitivity was due to the efficient adsorption of the target NH_3 gas molecules on the surfaces of the nanoflower−like MoS_2 sensitive layer, which had a larger specific surface area and provided more active sites, resulting in a more significant change in the resonant frequency of the device due to the mass loading effect.

Author Contributions: Conceptualization, C.-Y.C. and Y.-C.C.; methodology, C.-Y.C.; Formal analysis, C.-Y.C., K.-S.K. and E.-I.L.; Resources, Y.-C.C., K.-S.K. and F.-R.J.; Data curation, C.-Y.C.; Writing—original draft preparation, C.-Y.C.; Writing—review and editing, K.-S.K. and Y.-C.C.; Supervision, Y.-C.C.; Funding acquisition, C.-Y.C. All authors have read and agreed to the published version of the manuscript.

Funding: This research received no external funding.

Institutional Review Board Statement: Not applicable.

Informed Consent Statement: Not applicable.

Data Availability Statement: Not applicable.

Conflicts of Interest: The authors declare no conflict of interest.

References

1. Kampa, M.; Castanas, E. Human health effects of air pollution. *Environ. Pollut.* **2008**, *2*, 362–367. [CrossRef] [PubMed]
2. Clappier, A.; Thunis, P.; Beekmann, M.; Putaud, J.; de Meij, A. Impact of SOx, NOx and NH_3 emission reductions on PM2. 5 concentrations across Europe: Hints for future measure development. *Environ. Int.* **2021**, *156*, 106699. [CrossRef]
3. Zhou, Y.; Li, X.; Wang, Y.; Tai, H.; Guo, Y. UV Illumination−enhanced molecular ammonia detection based on a ternary−reduced graphene oxide–titanium dioxide–Au composite film at room temperature. *Anal. Chem.* **2018**, *5*, 3311–3318. [CrossRef] [PubMed]
4. Zhang, D.; Yang, Z.; Li, P.; Pang, M.; Xue, Q. Flexible self−powered high−performance ammonia sensor based on Au−decorated $MoSe_2$ nanoflowers driven by single layer MoS_2−flake piezoelectric nanogenerator. *Nano Energy* **2019**, *65*, 103974. [CrossRef]
5. Li, H.-Y.; Lee, C.-S.; Kim, D.H.; Lee, J.-H. Flexible room−temperature NH_3 sensor for ultrasensitive, selective, and humidity−independent gas detection. *ACS Appl. Mater. Interfaces* **2018**, *33*, 27858–27867. [CrossRef]

6. Kumar, A.; Sanger, A.; Kumar, A.; Chandra, R. Fast response ammonia sensors based on TiO_2 and NiO nanostructured bilayer thin films. *RSC Adv.* **2016**, *81*, 77636–77643. [CrossRef]
7. Van Toan, N.; Hung, C.M.; Van Duy, N.; Hoa, N.D.; Le, D.T.T.; Van Hieu, N. Bilayer SnO_2–WO_3 nanofilms for enhanced NH_3 gas sensing performance. *Mater. Sci. Eng. B* **2017**, *224*, 163–170. [CrossRef]
8. Li, P.; Wang, B.; Qin, C.; Han, C.; Sun, L.; Wang, Y. Band−gap−tunable CeO_2 nanoparticles for room−temperature NH_3 gas sensors. *Ceram. Int.* **2020**, *11*, 19232–19240. [CrossRef]
9. Perrozzi, F.; Emamjomeh, S.M.; Paolucci, V.; Taglieri, G.; Ottaviano, L.; Cantalini, C. Thermal stability of WS_2 flakes and gas sensing properties of WS_2/WO_3 composite to H_2, NH_3 and NO_2. *Sens. Actuators B Chem.* **2017**, *243*, 812–822. [CrossRef]
10. Yan, W.; Hu, M.; Wang, D.; Li, C. Room temperature gas sensing properties of porous silicon/V_2O_5 nanorods composite. *Appl. Surf. Sci.* **2015**, *346*, 216–222. [CrossRef]
11. Chen, X.; Zhao, S.; Zhou, P.; Cui, B.; Liu, W.; Wei, D.; Shen, Y. Room−temperature NO_2 sensing properties and mechanism of CuO nanorods with Au functionalization. *Sens. Actuators B Chem.* **2021**, *328*, 129070. [CrossRef]
12. Jakubik, W.; Powroźnik, P.; Wrotniak, J.; Krzywiecki, M. Theoretical analysis of acoustoelectrical sensitivity in SAW gas sensors with single and bi−layer structures. *Sens. Actuators B Chem.* **2016**, *236*, 1069–1074. [CrossRef]
13. Rana, L.; Gupta, R.; Tomar, M.; Gupta, V. ZnO/ST−Quartz SAW resonator: An efficient NO_2 gas sensor. *Sens. Actuators B Chem.* **2017**, *252*, 840–845. [CrossRef]
14. Raj, V.B.; Tomar, M.; Nimal, A.; Sharma, M.U.; Gupta, V. Nano−crystalline SnO_2 thin film based surface acoustic wave sensor for selective and fast detection of NO_2 gas. *Adv. Sci. Lett.* **2014**, *5–6*, 1124–1128. [CrossRef]
15. Wang, S.-H.; Shen, C.-Y.; Lien, Z.-J.; Wang, J.-H. Nitric oxide sensing properties of a surface acoustic wave sensor with copper−ion−doped polyaniline/tungsten oxide nanocomposite film. *Sens. Actuators B Chem.* **2017**, *243*, 1075–1082. [CrossRef]
16. Jakubik, W.P. Surface acoustic wave−based gas sensors. *Thin Solid Films* **2011**, *520*, 986–993. [CrossRef]
17. Wang, W.; Liu, X.; Mei, S.; Jia, Y.; Liu, M.; Xue, X.; Yang, D. Development of a Pd/Cu nanowires coated SAW hydrogen gas sensor with fast response and recovery. *Sens. Actuators B Chem.* **2019**, *243*, 157–164. [CrossRef]
18. Akbari, E.; Jahanbin, K.; Afroozeh, A.; Yupapin, P.; Buntat, Z. Brief review of monolayer molybdenum disulfide application in gas sensor. *Phys. B Condens. Matter* **2018**, *545*, 510–518. [CrossRef]
19. Chava, R.K.; Do, J.Y.; Kang, M. Hydrothermal growth of two dimensional hierarchical MoS_2 nanospheres on one dimensional CdS nanorods for high performance and stable visible photocatalytic H_2 evolution. *Appl. Surf. Sci.* **2018**, *433*, 240–248. [CrossRef]
20. Bai, J.; Shen, Y.; Zhao, S.; Chen, Y.; Li, G.; Han, C.; Wei, D.; Yuan, Z.; Meng, F. Flower−like MoS_2 hierarchical architectures assembled by 2D nanosheets sensitized with SnO_2 quantum dots for high−performance NH_3 sensing at room temperature. *Sens. Actuators B Chem.* **2022**, *353*, 131191. [CrossRef]
21. Chung, C.-Y.; Chen, Y.-C.; Chung, C.-J.; Kao, K.-S. The photoluminescence responses of two−dimensional atomic layers of MoS_2 excited by surface acoustic wave device. *Mod. Phys. Lett. B* **2022**, *36*, 2241004. [CrossRef]
22. Tang, G.; Zhang, J.; Liu, C.; Zhang, D.; Wang, Y.; Tang, H.; Li, C. Synthesis and tribological properties of flower−like MoS_2 microspheres. *Ceram. Int.* **2014**, *40*, 11575–11580. [CrossRef]
23. Ballantine, D., Jr.; White, R.M.; Martin, S.J.; Ricco, A.J.; Zellers, E.; Frye, G.; Wohltjen, H. *Acoustic Wave Sensors: Theory, Design and Physico–Chemical Applications*; Elsevier: Amsterdam, The Netherlands, 1996.
24. Morgan, D. *Surface Acoustic Wave Filters: With Applications to Electronic Communications and Signal Processing*; Academic Press: Cambridge, MA, USA, 2010; p. 9.
25. Ricco, A.; Martin, S.; Zipperian, T. Surface acoustic wave gas sensor based on film conductivity changes. *Sens. Actuators* **1985**, *8*, 319–333. [CrossRef]
26. Penza, M.; Aversa, P.; Cassano, G.; Wlodarski, W.; Kalantar, K. Layered SAW gas sensor with single−walled carbon nanotube−based nanocomposite coating. *Sens. Actuators B Chem.* **2007**, *127*, 168–178. [CrossRef]
27. Tang, Y.-L.; Li, Z.-J.; Ma, J.-Y.; Su, H.-Q.; Guo, Y.-J.; Wang, L.; Du, B.; Chen, J.-J.; Zhou, W.; Yu, Q.-K. Highly sensitive room−temperature surface acoustic wave (SAW) ammonia sensors based on Co_3O_4/SiO_2 composite films. *J. Hazard. Mater.* **2014**, *280*, 127–133. [CrossRef]
28. Burman, D.; Raha, H.; Manna, B.; Pramanik, P.; Guha, P.K. Substitutional doping of MoS_2 for superior gas−sensing applications: A proof of concept. *ACS Sens.* **2021**, *6*, 3398–3408. [CrossRef]
29. Mak, K.F.; Lee, C.; Hone, J.; Shan, J.; Heinz, T.F. Atomically thin MoS_2: A new direct−gap semiconductor. *Phys. Rev. Lett.* **2010**, *105*, 136805. [CrossRef]
30. Wang, W.; Zhen, Y.; Zhang, J.; Li, Y.; Zhong, H.; Jia, Z.; Xiong, Y.; Xue, Q.; Yan, Y.; Alharbi, N.S. SnO_2 nanoparticles−modified 3D−multilayer MoS_2 nanosheets for ammonia gas sensing at room temperature. *Sens. Actuators B Chem.* **2020**, *321*, 128471. [CrossRef]
31. Sharma, S.; Kumar, A.; Kaur, D. Room temperature ammonia gas sensing properties of MoS_2 nanostructured thin film. In *AIP Conference Proceedings*; AIP Publishing LLC: Melville, NY, USA, 2018; p. 030261.
32. Liu, B.; Chen, L.; Liu, G.; Abbas, A.N.; Fathi, M.; Zhou, C. High−performance chemical sensing using Schottky−contacted chemical vapor deposition grown monolayer MoS_2 transistors. *ACS Nano* **2014**, *8*, 5304–5314. [CrossRef]
33. Wenbo, L.; Rong, Q.; Shangjun, Z.; Hong, J.; Cheng, S.; Yueqin, Z. MoS_2 with Different Morphologies: Preparation and Gas−sensing Property of NH_3. *J. Inorg. Mater.* **2022**, *37*, 1135–1140.

34. Constantinoiu, I.; Miu, D.; Viespe, C. Surface acoustic wave sensors for ammonia detection at room temperature based on SnO_2/Co_3O_4 bilayers. *J. Sens.* **2019**, *2019*, 8203810. [CrossRef]
35. Guo, Y.; Long, G.; Tang, Y.; Wang, J.; Tang, Q.; Zu, X.; Ma, J.; Du, B.; Torun, H.; Fu, Y. Surface acoustic wave ammonia sensor based on SiO_2–SnO_2 composite film operated at room temperature. *Smart Mater. Struct.* **2020**, *29*, 095003. [CrossRef]
36. Tang, Y.; Ao, D.; Li, W.; Zu, X.; Li, S.; Fu, Y.Q. NH_3 sensing property and mechanisms of quartz surface acoustic wave sensors deposited with SiO_2, TiO_2, and SiO_2-TiO_2 composite films. *Sens. Actuators B Chem.* **2018**, *254*, 1165–1173. [CrossRef]
37. Xu, X.; Zu, X.; Ao, D.; Yu, J.; Xiang, X.; Xie, W.; Tang, Y.; Li, S.; Fu, Y. NH_3-sensing mechanism using surface acoustic wave sensor with AlO (OH) film. *Nanomaterials* **2019**, *9*, 1732. [CrossRef]
38. Zhao, L.; Wang, R.; Cao, Q. Highly Sensitive Surface Acoustic Wave NH_3 Gas Sensor Based on TiO_2 Film. *Sens. Mater.* **2020**, *32*, 4111–4119. [CrossRef]